
Progressive Fusion for Multimodal Integration

Shiv Shankar, Laure Thompson, Madalina Fiterau

College of Information and Computer Science
University of Massachusetts
USA

{sshankar, laurejt, mfiterau}@cs.umass.edu

Abstract

Integration of multimodal information from various sources has been shown to boost the performance of machine learning models and thus has received increased attention in recent years. Often such models use deep modality-specific networks to obtain unimodal features which are combined to obtain “late-fusion” representations. However, these designs run the risk of information loss in the respective unimodal pipelines. On the other hand, “early-fusion” methodologies, which combine features early, suffer from the problems associated with feature heterogeneity and high sample complexity. In this work, we present an iterative representation refinement approach, called Progressive Fusion, which mitigates the issues with late fusion representations. Our model-agnostic technique introduces backward connections that make late stage fused representations available to early layers, improving the expressiveness of the representations at those stages, while retaining the advantages of late fusion designs. We test Progressive Fusion on tasks including affective sentiment detection, multimedia analysis, and time series fusion with different models, demonstrating its versatility. We show that our approach consistently improves performance, for instance attaining a 5% reduction in MSE and 40% improvement in robustness on multimodal time series prediction.

1 Introduction

Traditionally, research in machine learning has focused on different sensory modalities in isolation, but it is well recognized that human perception relies on the integration of information from multiple sensory modalities. Multimodal fusion research aims to fill this gap by integrating different unimodal representations into a unified common representation [Turchet et al., 2018, Baltrušaitis et al., 2018].

Typically, fusion techniques fall into two categories, *early fusion* and *late fusion*, depending on where the information from each modality is integrated in the feature pipeline [Varshney, 1997, Ramachandram and Taylor, 2017]. While theoretically early fusion models tend to be more expressive, in practice they are more commonly used for homogeneous or similar modalities [Ramachandram and Taylor, 2017]. On the other hand late fusion models are more effective in combining diverse modalities. This has generally been attributed to the challenges like feature shifts, cross-modal distributional changes, difference in dimensionality, etc. when dealing with heterogeneities across diverse modalities such as text and image [Mogadala et al., 2021, Yan et al., 2021].

In this work, we aim to bridge this divide by using backward connections which connect the late fused representation (à la late fusion) to unimodal feature generators and hence provide multimodal information at early layers (à la early fusion). This creates a model that learns to progressively refine the fused multimodal representations.

We show that our proposed technique called progressive-fusion (Pro-Fusion) results in improvements of different multimodal fusion architectures including recent *state of the art* models such as

MAGXLNET [Rahman et al., 2020], MIM [Han et al., 2021] and MFAS [Pérez-Rúa et al., 2019]. Our experiments show that training with the Pro-Fusion design results in more accurate and robust models compared to the initial state of the art architectures.

Contributions: (1) We propose a framework to bridge the gap between early and late fusion via backward connections. (2) We apply this model-agnostic approach to a broad range of state of the art models for a diverse set of tasks. (3) We show, through rigorous experiments, that models trained with Pro-Fusion are not just consistently more accurate, but also considerably more robust than the corresponding standard baseline models. We show up to 2% improvement in accuracy over state of the art sentiment prediction models and up to 5% reduction in MSE and 40% improvement in robustness on a challenging multimodal timeseries prediction task.

2 Preliminaries and Related Work

2.1 Multimodal Fusion

Multimodal learning is a specific type of supervised learning problem with different types of input modalities. We are provided with a dataset of N observations $\mathcal{D} = (X^j, Y^j)_{j=1}^N$, where all X^j come from a space \mathcal{X} and Y^j from \mathcal{Y} , and a loss function $L : \mathcal{Y} \times \mathcal{Y} \rightarrow \mathbb{R}$ which is the task loss. Our goal is to learn a parametric function $\mathcal{F} : \mathcal{X} \rightarrow \mathcal{Y}$ such that the total loss $\mathcal{L} = \sum_j L(\mathcal{F}(X^j), Y^j)$ is minimized. In multimodal fusion the space of inputs \mathcal{X} naturally decomposes into K different modalities $\mathcal{X} = \prod_{i=1}^K \mathcal{X}_i$. Correspondingly any observation X^j also decomposes into modality specific components X_i^j i.e. $X^j = (X_1^j, X_2^j, \dots, X_K^j)$.

A natural way to learn such a function with a multimodal input is to have an *embedding component* which fuses information into a high dimensional vector in \mathbb{R}^d , where d is the size of the embedding, and a *predictive component* P which maps the embedding vector from \mathbb{R}^d to \mathcal{Y} . Furthermore, since different modalities are often of distinct nature and cannot be processed by similar networks (e.g. text and image), the embedding generator is decomposed into (a) unimodal feature generators $G_i : \mathcal{X}_i \rightarrow \mathbb{R}^{d_i}$ which are specifically designed for each individual modality \mathcal{X}_i and (b) a fusion component $F : \prod_i \mathbb{R}^{d_i} \rightarrow \mathbb{R}^d$ which fuses information from each individual unimodal vector. F is provided with unimodal representations of the input X^j obtained through embedding networks G_i . The unimodal feature generators G_i can have different kinds of layers including 2D convolution, 3D convolution and fully connected layers. F is the layer where the embeddings obtained from different modalities are fused. F is called the *fusion* or *shared representation* layer. F has to capture both unimodal dependencies (i.e. relations between features that span only one modality) and multimodal dependencies (i.e. relationships between features across multiple modalities).

2.2 Prior Approaches to Fusion

In this section we provide a brief overview of late and early fusion, followed by a discussion of models used in this work. We present a more detailed discussion of related works in Appendix A.

Early Fusion and Late Fusion Early and Late Fusion is a broad categorization of fusion models in terms of how the fusion operation (layer where features from different modalities are combined) splits the complexity of the model [Ayache et al., 2006, Ramachandram and Taylor, 2017]. Early fusion (Figure 1a) combines the modalities 'early' and devotes more model complexity to post fusion operations. In contrast to early fusion, late fusion design (Figure 1b), has significantly more unimodal processing and combines the features from different modalities 'late'. Early fusion models have the ability to model highly complex dependencies between different modalities, but face problems when dealing with heterogeneous sources such as text and images. Late fusion allows an easy way to aggregate information from diverse modalities and run the risk of missing cross-modal interactions in the mixed feature space.

Architecture Changes Many recent works including that of Vielzeuf et al. [2018], Sankaran et al. [2021], Pérez-Rúa et al. [2019], Hazarika et al. [2020] design new deep architectures. Vielzeuf et al. [2018] proposed a CentralNet design based on aggregative multi-task learning. Sankaran et al. [2021] design a Refiner Fusion Network (Refnet) trained via cyclic losses. Pérez-Rúa et al. [2019] used neural architecture search to find a good architecture for convolutional networks. Hsu and Glass [2018] and Khattar et al. [2019] use multimodal autoencoders to learn better representations. Tsai

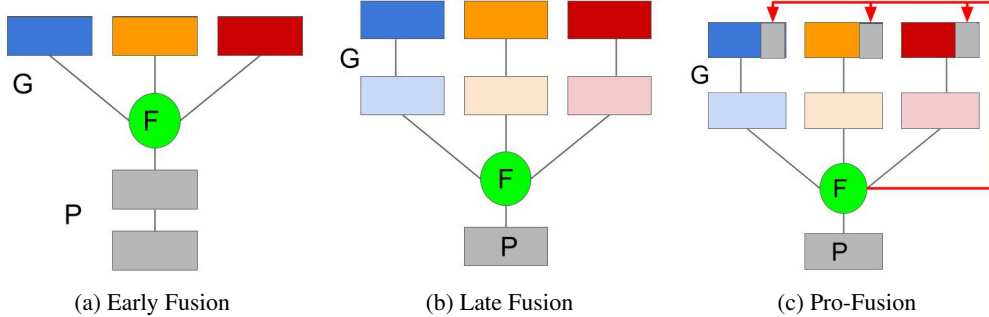


Figure 1: Representative Multimodal Fusion Architectures of a) Early fusion , b) Late fusion and c) Pro-Fusion. We have also indicated the components mentioned in Section 2.1 viz. the unimodal feature generators G , fusion layer F and predictive network P in the figures. Generally models with high capacity P/G are considered early/late fusion respectively. The key difference between a late fusion architecture and pro-fusion architecture are the skip-back connections, indicated in red.

et al. [2019b] improved upon the factor model based approach of Hsu and Glass [2018]. Nagrani et al. [2021] modify the multimodal transformer [Tsai et al., 2019a] to incorporate bottlenecks.

Our proposed method, though technically an architecture change, is a single change that *treats the existing model as given*. It is closer in spirit to a black-box change, compared to the aforementioned methods. Hence it is *complementary* to this line of work. We experiment with many of the aforementioned models to show how our proposal consistently improves performance.

Fusion Techniques Other than basic fusion layers such as pooling and concatenation, other common layers use include aggregation [Khan et al., 2012], tensor factorisation [Liu et al., 2018, Zadeh et al., 2017], attention [Tsai et al., 2019a] and memory modules [Zadeh et al., 2018a]. Rahman et al. [2020] design a model using pre-trained transformer to achieve state of the art results on the multimodal sentiment benchmarks. These works propose specific fusion techniques, they design specific forms of the F function (see Figure 1). Our proposed technique is *agnostic to the choice of the fusion function F* and thus is *orthogonal* to these ideas.

Model Agnostic Methods Model independent methods to improve fusion by using train-time objectives based on cortical synergy [Shankar, 2021], mutual information [Bramon et al., 2011], or contrastive estimation [Liu et al., 2021] have been explored. Recently Wang et al. [2020a] proposed a reweighing based approach (GB) to tackling the problem of jointly learning models of differing capacity. Sohn et al. [2014], Suzuki et al. [2016] have proposed generative approaches for capturing cross-modal interactions between features. Our proposal is distinct from these methods in that it adds backprojective connections. These model-agnostic proposals are generally orthogonal to our approach, and potentially can be combined to *achieve further improvements*. For example, in our experiments we will show that our method can increase performance on GB based models as well.

3 Progressive Fusion (Pro-Fusion)

3.1 Motivating Example

Consider the task of determining the location of an entity from video and text. For instance, suppose the system has to detect the coordinates, in a given image, of an object specified through a textual command. For the image provided in Figure 2, the text might be ‘find the tennis ball’ or ‘find the blue bone’. The task is not solvable using a single modality, as the image only contains the objects and their location, whereas the text only contains information about the object of interest.



Figure 2: Example image for motivating case. The target corresponds to the location in the image of the object described in the audio modality (dog, ball, bone etc). Source: <https://kylekittleson.com/>.

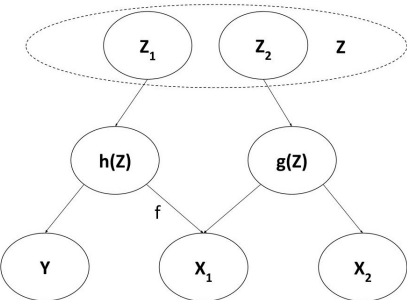


Figure 3: Generative Model for the case discussed in Section 3.1. Z is the latent variable that determines the outcome Y via $h(Z)$. $g(Z)$ is a function of Z independent of Y . X_1 is a combination of $h(Z)$ and $g(Z)$.

Now consider what might happen with a late-fusion scheme. A significant part of the representation capacity of the image features might be devoted to capturing the dog, the bone, the carpet etc. And hence determining the coordinates of the small tennis ball will be more challenging unless the image feature generator has access to the textual information. More generally, if the unimodal feature generators are bottlenecked or not powerful enough; the required information to predict the output might be lost or compressed too much to be recovered correctly. With early fusion, the image feature generator knows which object to focus on and can be directed towards the relevant information, specifically the location and other information about the tennis ball.

Figure 3 represents an abstract graphical model for this situation. X_1 represents the entire input image, while Z represents an abstract state of the environment (with objects and coordinates). The output Y (e.g. coordinate target) is determined by the feature function h so $Y \leftarrow h(z)$ (i.e. $h(Z)$ contains sufficient statistics about the location of the object). The information about these features are present in X_1 (obtained by applying unknown function f to $h(Z)$); however X_1 has nuisance variables (e.g. other objects) or a corrupted version of $h(z)$. $g(Z)$ represents descriptions like colour, shape etc of the target object. The location $h(Z)$ and visual characters $g(Z)$ put together forms (part of) the image. In this case Y may not be identifiable purely via X_1 . For the image example, this is because X_1 has not just the target but other objects which means the without characterizing the desired target, a specific location cannot be specified. But in the presence of input X_2 (in this case text) the target is identifiable even if X_2 by itself is not informative about Y .¹

In such a scenario, with late fusion based approach if the encoder G_1 (unimodal feature generator for mode \mathcal{X}_1) is not sufficiently powerful, the overall networks may not be able to learn the perfect function f even in the presence of modality \mathcal{X}_2 . This can happen during late fusion when the network F_1 has already pooled together h and g in a non-invertible manner. On the other hand if the features from X_2 were made available to the feature encoder for X_1 , it can learn to ignore or mask nuisance variation/corruption. This however requires the model to perform some form of early fusion; but if the underlying modalities \mathcal{X}_2 and \mathcal{X}_1 are very different, the corresponding integration is challenging.

This leads us to our basic problem. We aim to design a generic approach that combines the advantages of late and early fusion. To this end, we propose a model agnostic scheme based on providing late multi-modal fusion features to unimodal feature generators.

3.2 Pro-Fusion

We build a scheme based on backprojective connections which can be applied to any given base architecture. Our scheme considers any given base design as a single step of an iterative process. The base design is augmented to take an additional context vector as input, which serves to provide information from 'late' fused representations. At each iteration, the current output representations of the base model are provided via the context vector as an additional input for the next step. More formally, given a base model \mathcal{F} with input $x = (x_i, x_2, \dots, x_k)$, we want to create an augmented model

¹For an example in terms of equations refer to Appendix B.1

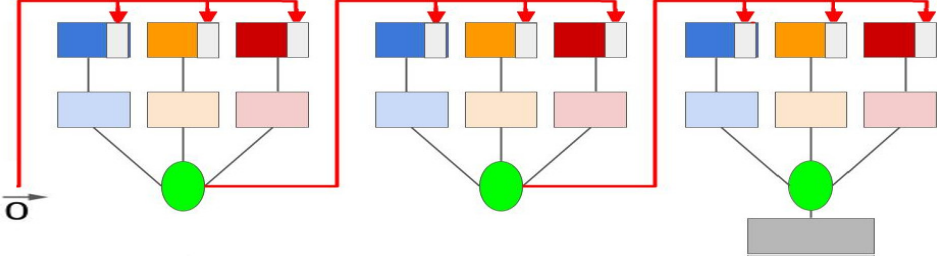


Figure 4: Example Pro-Fusion design unrolled for 3 steps with the Late Fusion Model (Figure 1b).

$\hat{\mathcal{F}} : \mathcal{X} \times \mathbb{R}^d \rightarrow \mathcal{Y}$ with additional input $c \in \mathbb{R}^d$ such that $c = 0 \implies \hat{\mathcal{F}}(x, c) = \mathcal{F}(x)$. Recall that the function \mathcal{F} mentioned in Section 2.1 is given by $\mathcal{F}(x) = P(F(G_1(x_1), G_2(x_2), \dots G_K(x_K)))$.

We create the desired network $\hat{\mathcal{F}}$ by providing c to the unimodal feature generators G_j . We use the output of the fusion layer F and project it back into the network as c_t via the matrix/function W_i . This creates an iterative network which we run for R steps. The final vector c_R after R steps serves as the output of fusion which is then provided to the predictor model P .

Figure 1c shows an example in which back-projecting connection have been added to the Late Fusion Base Model in Figure 1b. In Figure 4 we visually depict how the model is unrolled.

The ability to send information backward in the network addresses the problem raised earlier in Section 3.1. The encoder G_1 for X_1 can now gain a handle on $g(Z)$ via the fused output c_1 . Specifically if the model can compute $g(z)$ from $W(c_1)$, then in the second iteration step, one can recover from X_2 the real value of $h(Z)$, which then directly determines the target Y . On the other hand if X_2 is not useful or if G_1 cannot process the fused vector efficiently, then $W(\cdot)$ can be zeroed out and the overall model is no worse than the baseline model. We also present in the Appendix E, some mathematical analysis as to the representation power of our approach.

A reader might notice some similarities to memory based fusion methods [Gammulle et al., 2017, Zadeh et al., 2018a,b]. However there are two important differences. Firstly, the purpose of memory in those methods is retaining history for easier learning of interactions across time steps in a sequential input. On the other hand, in our proposal, context vector serves the purpose of making late-fusion features accessible to the unimodal network processing models/early stage features. Our proposal is entirely independent of any temporal axis/sequential nature in the input. Secondly, these methods capture historical relationships only in unimodal data, and memory is used directly over the concatenated unimodal features. On the other hand our approach provides multimodal information to unimodal feature generators.

4 Experiments

In this section, we empirically demonstrate that Pro-Fusion improves performance of multimodal deep learning SOTA architectures on a variety of tasks. First we verify our intuition for the advantage of backward connections in a synthetic experiment. Next we experiment with datasets in sentiment prediction [Zadeh et al., 2018b], multimedia classification [Vielzeuf et al., 2018] and financial timeseries prediction [Sardelich and Manandhar, 2018]. We also explore how our approach affects robustness for noisy time series data. Finally we evaluate the impact of varying the number of unrolling steps and analyze how the model performance as well as unimodal representations evolve. For all the datasets we use SOTA and near-SOTA models, while keeping a diversity of fusion techniques and network designs. For each dataset and architecture combination, we either use established hyperparameters and/or choose the best hyperparameter from our own experiments. Next for the same architecture, we *add backward connections* from the fusion layer output and train with the exact same hyperparameters. We *do not perform any hyperparameter tuning or search for our modified models*, so the reported results are a lower bound on what Pro-Fusion can achieve. We opt for this process to isolate the effects of adding backward connections from those of tuning hyperparameters.

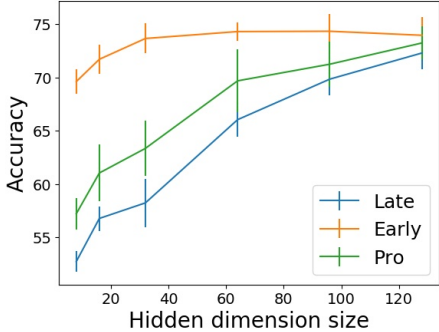


Figure 5: Accuracy of late, early and pro-fusion models over varying levels of inner dimension. Each point corresponds to the performance of the corresponding model when the hidden dimension is set to the values of d on the x axis.

| Model | Accuracy \uparrow | |
|--------|---------------------|-------------|
| | Base | Ours |
| LF | 71.4 | 71.6 |
| LFN | 71.1 | 71.8 |
| MFM | 71.4 | 72.2 |
| GB | 68.9 | 69.3 |
| Refnet | 70.6 | 71.2 |
| MFAS | 72.1 | 72.5 |
| MBT | 70.3 | 70.3 |

Table 1: Results on digit classification task with AVMNIST for various fusion architectures. The performance metric is Accuracy, and was measured on five trials. Our method *outperforms the baseline in almost all instances*. Scores above 1 standard deviation of the base models, indicating significance, have been highlighted.

4.1 Synthetic Dataset

To verify the intuition described in Section 3.1, we first create a synthetic experiment. For this purpose in modality $\mathcal{X}_1 \subset \mathbb{R}^D$ we encode a smooth random function. Specifically the d^{th} component of X_1 has the value of the function at the point d/D . Next in modality \mathcal{X}_2 , we provide position embeddings of a randomly chosen lattice point $l \in \{0, 1/D, 2/D, \dots, 1\}$. The output label Y is the first non-zero digit of x_l . This is conceptually a simple task as one can infer the component from the modality \mathcal{X}_2 and simply read on the corresponding component from \mathcal{X}_1 . However if the model is late fusion, where the input modalities might go through a lower dimensional representation; the specific values of each component in \mathcal{X}_1 is lost, and the model cannot correctly predict the label. Note that in this case, each instance of \mathcal{X}_1 must contain a different function; as if the function was fixed the network can try to directly learn the function itself instead of looking at the input.

In Figure 5, we plot the accuracy of a 2 layer MLP trained on this task with different sizes of hidden layer. The argument from Section 3.1 suggests that early fusion is more effective than late fusion when the hidden layers are smaller. Furthermore it also suggests that the effect of progressive fusion is larger when the feature layers input to late fusion is smaller. This comes out in the experiments, where the gap between pro-fusion model and late fusion model reduces as the hidden representation becomes larger. Finally for a large enough hidden representation, the performance of late fusion matches that of early fusion. More analysis on synthetic settings are presented in Appendix B.1

4.2 Multimedia Classification

Datasets. We first evaluate our proposed design changes on AV-MNIST [Vielzeuf et al., 2018], a popular benchmark dataset used for multimodal fusion [Pérez-Rúa et al., 2019, Joze et al., 2020]. It is an audio-visual dataset for a digit classification task. The data is prepared by pairing human utterances of digits obtained from FSDD dataset² with images of written digits from MNIST. This dataset has 55K training, 5K validation, and 10K testing examples. To prepare the dataset we use the processing stack of Cassell [2019]. The preprocessing involves adding corruption to both modalities, so that no single modality is enough by itself for the task [Vielzeuf et al., 2018].

Models. **LF** is the baseline late fusion architecture used in Vielzeuf et al. [2018]. **MFAS** is the architecture search based model used by Pérez-Rúa et al. [2019]. It is the current SOTA on AV-MNIST. The exact architecture is presented in the Appendix D.3. We use the model obtained by search and add the backward connections. **LFN** is the low rank tensor fusion approach [Zadeh et al., 2017] adapted to this dataset, while **MFM** refers to the factorization method of Tsai et al. [2019b] for learning multimodal representation. **GB** and **Refnet** are the gradient blending and refiner network based approaches of Wang et al. [2020a] and Sankaran et al. [2021] respectively. **MBT** is the multimodal transformer model of Nagrani et al. [2021]. Similar to existing work [Vielzeuf et al.,

²https://www.tensorflow.org/datasets/catalog/spoken_digit

| Dataset | MOSEI | | | | MOSI | | | |
|----------|------------------|-------------|------------------|-------------|------------------|-------------|------------------|-------------|
| | $Acc_7 \uparrow$ | | $Acc_2 \uparrow$ | | $Acc_7 \uparrow$ | | $Acc_2 \uparrow$ | |
| Model | Base | Ours | Base | Ours | Base | Ours | Base | Ours |
| FLSTM | 44.1 | 44.8 | 75.1 | 75.8 | 31.2 | 31.8 | 75.9 | 76.8 |
| LFN | 44.9 | 46.1 | 75.3 | 76.4 | 31.2 | 32.1 | 76.6 | 77.2 |
| MAGBERT | 46.9 | 47.1 | 83.1 | 83.6 | 40.2 | 40.8 | 83.7 | 84.1 |
| MAGXLNET | 46.7 | 47.1 | 83.9 | 84.2 | 43.1 | 43.5 | 85.2 | 85.5 |
| MIM | 53.3 | 54.1 | 79.1 | 80.1 | 45.5 | 46.3 | 81.7 | 83.4 |

Table 2: Results on sentiment analysis on CMU-MOSEI. Acc_7 and Acc_2 denote accuracy on 7 and 2 classes respectively

2018, Liang et al., 2021a] our experiments used the aforementioned fusion designs with unimodal LeNet style feature generators, except for MBT which uses transformers.

Our results are presented in Table 1. Amongst all the methods we evaluated, Pro-MFAS was the best model and beats its standard counterpart by 0.4 accuracy points. We also observe similar improvements in using Pro-Fusion with the MFM design. In fact the Pro-fusion MFM model was competitive with the current state of the art MFAS model. Meanwhile, gradient blending (GB) based fusion approach seems to not generalize on this dataset and performs worse than even the baseline late fusion method.

4.3 Sentiment Prediction

Datasets. We empirically evaluate our methods on two datasets CMU-MOSI [Wöllmer et al., 2013] and CMU-MOSEI [Zadeh et al., 2018b]. CMU-MOSI is sentiment prediction tasks on a set of short youtube video clips. CMU-MOSEI is a similar dataset consisting of around 23k review videos taken from YouTube. Both of these are used generally for multimodal sentiment analysis experiments. For each dataset, three modalities are available: audio, video, and language.

Models. **FLSTM** is the early fusion type baseline LSTM architecture used by Zadeh et al. [2017], while **LFN** is the low rank tensor representation of model of Zadeh et al. [2017]. multimodal features. [Hazarika et al., 2020]. **MAGBERT** and **MAGXLNET** [Rahman et al., 2020] are BERT [Devlin et al., 2018] based state of the art models on these datasets. These architectures uses a gating mechanism [Wang et al., 2019] to augment a pretrained transformer. **MIM** [Han et al., 2021] is a recent near state of the art architecture. It combines BERT based text embeddings with modality specific LSTMs.

We evaluate our change on the aforementioned five models on four metrics commonly used in the literature [Zadeh et al., 2017, Han et al., 2021]. We use two classification-based measures, namely, binary accuracy and more fine-grained 7-class accuracy; and two regression measures, namely, mean average error (MAE) and correlation (CORR) between predicted and actual scores. The accuracy results are reported in Table 2. We present the results of the remaining metrics in Appendix 6. We observe consistent improvements in accuracy of non-transformer based models (FLSTM, LFM, MIM) ranging from 0.5% to 1.5%, while transformer based models improve by 0.3%. The comparatively smaller improvement in transformers could be due to the lack of additional information from other modalities when using transformers on text. For example, on CMU-MOSI simply using BERT embeddings provides an accuracy of 78% which is higher than most non-BERT fusion models [Hazarika et al., 2020]. Given the high degree of sufficiency in the textual modality, performance improvement is mainly determined by the text processing network, more so than by the fusion design.

4.4 Financial Data

Datasets. We evaluate our approach on a multimodal financial time series prediction task [Sardelich and Manandhar, 2018]. F&B, HEALTH, and TECH are prices and events related to publically listed companies organized according to the primary business sector. Within each sector, historical prices are used as time series inputs to predict the future price and volatility of a related stock. In this setting the different stocks in the same sector correspond to different modalities. Due to the significantly large number of available modalities, this task presents a different set of challenges [Emerson et al., 2019, Sardelich and Manandhar, 2018] than other datasets. Moreover, due to the inherently low

signal-to-noise ratio in such time series, it presents a greater robustness challenge than other datasets [Liang et al., 2021a]. On the other hand, due to the similar nature of the modalities this task is amenable to a variety of early fusion methods.

Models. We experiment with Transformers for time series [Sardelich and Manandhar, 2018] with both early fusion **EF transf** and late fusion **LF transf** variants. The other models we test are the multimodal fusion transformer **MuLT** Tsai et al. [2019a], Gradient Blending **GB** approach from [Wang et al., 2020a]. Finally as LSTMs are strong baselines on this task [Narayanan et al., 2019], we also use Early fusion **EFLSTM** and Late **LFLSTM** fusion LSTM models.

| Model | Metric | MSE ↓ | | Robustness ↑ | |
|-----------|--------|---------|--------------|--------------|-------------|
| | | Dataset | Base | Ours | Base |
| EFLSTM | F&B | 0.73 | 0.70 | 0.87 | 1.0 |
| | HEALTH | 0.308 | 0.306 | 0.54 | 0.83 |
| | TECH | 0.742 | 0.738 | 0.92 | 0.93 |
| LFLSTM | F&B | 0.77 | 0.73 | 0.74 | 0.83 |
| | HEALTH | 0.331 | 0.315 | 0.48 | 0.78 |
| | TECH | 0.736 | 0.737 | 0.96 | 0.96 |
| GB | F&B | 0.690 | 0.688 | 0.98 | 0.98 |
| | HEALTH | 0.318 | 0.305 | 0.67 | 1.0 |
| | TECH | 0.740 | 0.728 | 0.99 | 1.0 |
| LF Transf | F&B | 0.838 | 0.788 | 0.24 | 0.38 |
| | HEALTH | 0.337 | 0.331 | 0.34 | 0.46 |
| | TECH | 0.757 | 0.751 | 0.92 | 0.93 |
| MuLT | F&B | 0.814 | 0.765 | 0.33 | 0.48 |
| | HEALTH | 0.333 | 0.329 | 0.0 | 0.08 |
| | TECH | 0.763 | 0.757 | 0.85 | 0.86 |
| EF Transf | F&B | 0.836 | 0.827 | 0.0 | 0.05 |
| | HEALTH | 0.335 | 0.326 | 0.45 | 0.63 |
| | TECH | 0.755 | 0.750 | 0.0 | 0.0 |

Table 3: Results on stock prediction on the three sectoral datasets. The performance is evaluated on the Mean Squared Error (MSE) metric evaluated on 10 trials. We also compute robustness metrics by testing on data corrupted with various noise levels and present the relative robustness scores. Scores which are outside the 1 standard deviation of the base model are highlighted.

Because of the similar nature of the modalities one might expect early fusion based models to be effective. This can be seen in our results where early fusion LSTM outperforms late fusion models. However, we note that, by using backward connections, the late fusion models, especially LFLSTM, become competitive with early fusion models. The nature of the dataset—low dimension time series with inherent noise—means we can also assess the robustness of the models against modality corruption easily. We add varying levels of noise to the test data and see how the performance of the models change with increasing noise. Following [Taori et al., 2020, Shankar et al., 2017, Liang et al., 2021a] the robustness of the model is assessed by computing the area under the performance vs noise curve. Specifically it is computed by discrete approximation of the following integral:

$$\tau = \int \text{MSE}(f, \sigma) - \text{MSE}(b, \sigma) d\sigma$$

where $\text{MSE}(\cdot, \sigma)$ is the MSE of the model on test-data with inputs corrupted with noise level σ . f is the model the evaluated and b is a baseline model. We choose late fusion transformer as our baseline, and scale the numbers between 0 and 1³. From the results we can see that *Pro-fusion provides greater improvements on late fusion compared to early fusion designs*. This suggests that part of the improvement is due to backward connection based fusion acting as a bridge between early and late fusion designs.

4.5 Exploring the representations

Next, we analyze how the unimodal representations evolve over the unrolling steps. For this purpose, we consider the activations of unimodal networks \hat{G}_j (equivalently, the inputs for the late fusion layer) as the unimodal representations. For these of experiments, we use LFN, MFM and Refnet models on AVMNIST. We train a linear classifier based on the unimodal representations from the training data and find its accuracy on the test data.

In Figure 6 we plot the relative test accuracy of both the audio and image features against the iteration number for all the models. We can see gains in all models after one step of unrolling. Since we know that individual modalities are quite incomplete on AVMNIST (< 60% accuracy on individual modalities) and the accuracy of only image modality at the first step is close to 60%. This suggests

³For the unscaled value of the numbers refer to Appendix C

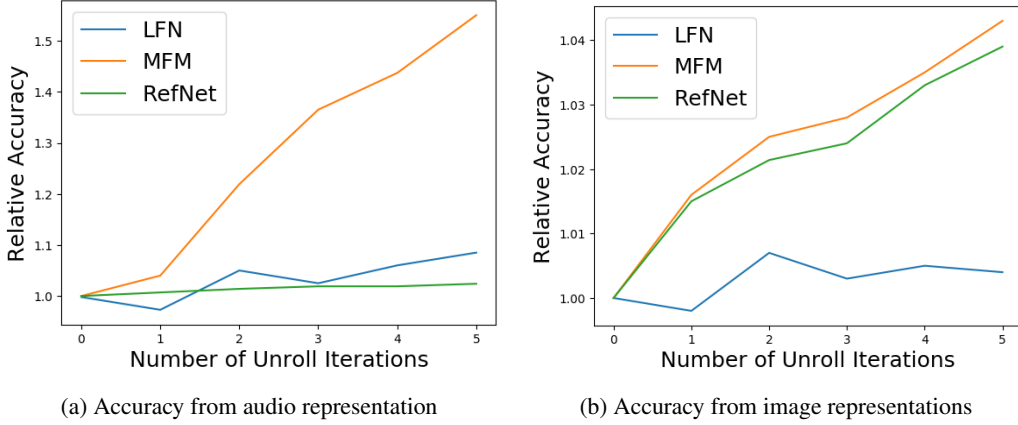


Figure 6: Behavior of classifiers trained on the unimodal embedding against number of unrolling iterations. We train a linear model on the input to the fusion layer and on them. The lines plot the normalized accuracy of the trained model. We observe *increased accuracy* with more unrolling.

that the unimodal modalities are now integrating information from each other. Along with the overall trend, this suggests that *the model is incorporating more multimodal information in each unimodal representation*.

5 Conclusion

Our paper presents a model-agnostic approach to incorporate benefits of early fusion into late fusion networks via backward connections. We argued for some sufficient conditions when our backward connection based design to be more effective than usual fusion designs, supported by an artificial data experiment. Through thorough experiments, we made a case for using backward connections to improve model performance and robustness. We showed that Pro-fusion led to performance improvements even on SOTA architecture, which opens new research avenues in exploring options for backprojection of information in multimodal fusion architectures.

Limitations and Social Impact Multimodal fusion is an important problem in health-care application. Improvements in early identification of conditions such as Alzheimer’s, using information from health records, can add significantly to the quality of life for patients. A future potential direction of our work is to assess its applicability in healthcare domain. Our experiments do not give a clear answer to the question of how our approach interacts with other model agnostic methods. However as the processing induced by ProFusion is similar to message passing on the graph in Figure 3, if the task has a similar dependency structure between modalities, then our method can be expected to yield good improvements⁴ That said, no model design is suitable for all problems, and our results are limited to the datasets we experimented on.

References

- M. Abavisani, H. R. V. Jozé, and V. M. Patel. Improving the performance of unimodal dynamic hand-gesture recognition with multimodal training. In *Proceedings of the IEEE/CVF Conference on Computer Vision and Pattern Recognition*, pages 1165–1174, 2019.
- S. Ayache, G. Quénot, J. Gensel, and S. Satoh. Using topic concepts for semantic video shots classification. In *Proceedings of the 5th International Conference on Image and Video Retrieval, CIVR’06*. Springer-Verlag, 2006. ISBN 3540360182.
- T. Baltrušaitis, C. Ahuja, and L.-P. Morency. Multimodal machine learning: A survey and taxonomy. *IEEE transactions on pattern analysis and machine intelligence*, 41(2):423–443, 2018.

⁴for details refers to Appendix G

R. Bramon, I. Boada, A. Bardera, J. Rodriguez, M. Feixas, J. Puig, and M. Sbert. Multimodal data fusion based on mutual information. *IEEE Transactions on Visualization and Computer Graphics*, 18(9):1574–1587, 2011.

L. Cabrera-Quiros, D. M. Tax, and H. Hung. Gestures in-the-wild: Detecting conversational hand gestures in crowded scenes using a multimodal fusion of bags of video trajectories and body worn acceleration. *IEEE Transactions on Multimedia*, 22(1):138–147, 2019.

S. Cassell. Mfas. https://github.com/slyviacassell/_MFAS/, 2019.

Z. Chair and P. Varshney. Optimal data fusion in multiple sensor detection systems. *IEEE Transactions on Aerospace and Electronic Systems*, (1):98–101, 1986.

J. Devlin, M.-W. Chang, K. Lee, and K. Toutanova. Bert: Pre-training of deep bidirectional transformers for language understanding. *arXiv preprint arXiv:1810.04805*, 2018.

S. Emerson, R. Kennedy, L. O’Shea, and J. O’Brien. Trends and applications of machine learning in quantitative finance. In *8th international conference on economics and finance research (ICEFR 2019)*, 2019.

H. Gammulle, S. Denman, S. Sridharan, and C. Fookes. Twin memory lstm: deep fusion framework for human action recognition. 2017.

W. Han, H. Chen, and S. Poria. Improving multimodal fusion with hierarchical mutual information maximization for multimodal sentiment analysis. In *Proceedings of EMNLP 2021*, 2021.

D. Hazarika, R. Zimmermann, and S. Poria. Misa: Modality-invariant and-specific representations for multimodal sentiment analysis. In *Proceedings of the 28th ACM International Conference on Multimedia*, pages 1122–1131, 2020.

J.-C. Hou, S.-S. Wang, Y.-H. Lai, Y. Tsao, H.-W. Chang, and H.-M. Wang. Audio-visual speech enhancement based on multimodal deep convolutional neural network. *arXiv preprint arXiv:1709.00944*, 2017.

W.-N. Hsu and J. Glass. Disentangling by partitioning: A representation learning framework for multimodal sensory data. *arXiv preprint arXiv:1805.11264*, 2018.

J. Hu, L. Shen, S. Albanie, G. Sun, and E. Wu. Squeeze-and-excitation networks, 2019.

H. R. V. Joze, A. Shaban, M. L. Iuzzolino, and K. Koishida. Mmtm: Multimodal transfer module for cnn fusion. In *Proceedings of the IEEE/CVF Conference on Computer Vision and Pattern Recognition*, pages 13289–13299, 2020.

F. S. Khan, R. M. Anwer, J. Van De Weijer, A. D. Bagdanov, M. Vanrell, and A. M. Lopez. Color attributes for object detection. In *2012 IEEE Conference on Computer Vision and Pattern Recognition*, pages 3306–3313. IEEE, 2012.

D. Khattar, J. S. Goud, M. Gupta, and V. Varma. Mvae: Multimodal variational autoencoder for fake news detection. In *The world wide web conference*, pages 2915–2921, 2019.

D. Koller and N. Friedman. *Probabilistic graphical models: principles and techniques*. MIT press, 2009.

X. Li and E. Seignez. Driver inattention monitoring system based on multimodal fusion with visual cues to improve driving safety. *Transactions of the Institute of Measurement and Control*, 40(3):885–895, 2018.

P. Liang, Y. Lyu, X. Fan, Z. Wu, Y. Cheng, J. Wu, L. Chen, P. Wu, M. Lee, Y. Zhu, et al. Multibench: Multiscale benchmarks for multimodal representation learning. 2021a.

T. Liang, G. Lin, L. Feng, Y. Zhang, and F. Lv. Attention is not enough: Mitigating the distribution discrepancy in asynchronous multimodal sequence fusion. In *Proceedings of the IEEE/CVF International Conference on Computer Vision*, pages 8148–8156, 2021b.

P. Liu, S. Chang, X. Huang, J. Tang, and J. C. K. Cheung. Contextualized non-local neural networks for sequence learning. In *Proceedings of the AAAI Conference on Artificial Intelligence*, volume 33, pages 6762–6769, 2019.

Y. Liu, Q. Fan, S. Zhang, H. Dong, T. Funkhouser, and L. Yi. Contrastive multimodal fusion with tupleinfonce. In *Proceedings of the IEEE/CVF International Conference on Computer Vision (ICCV)*, pages 754–763, October 2021.

Z. Liu, Y. Shen, V. B. Lakshminarasimhan, P. P. Liang, A. Zadeh, and L.-P. Morency. Efficient low-rank multimodal fusion with modality-specific factors. *arXiv preprint arXiv:1806.00064*, 2018.

A. Mogadala, M. Kalimuthu, and D. Klakow. Trends in integration of vision and language research: A survey of tasks, datasets, and methods. *Journal of Artificial Intelligence Research*, 2021.

A. Nagrani, S. Yang, A. Arnab, A. Jansen, C. Schmid, and C. Sun. Attention bottlenecks for multimodal fusion. *Advances in Neural Information Processing Systems*, 34, 2021.

A. Narayanan, A. Siravuru, and B. Dariush. Temporal multimodal fusion for driver behavior prediction tasks using gated recurrent fusion units. *CoRR*, abs/1910.00628, 2019. URL <http://arxiv.org/abs/1910.00628>.

L. Osadciw and K. Veeramachaneni. *Fusion, Decision-Level*. Springer US, 2009.

J.-M. Pérez-Rúa, V. Vielzeuf, S. Pateux, M. Baccouche, and F. Jurie. Mfas: Multimodal fusion architecture search. In *Proceedings of the IEEE/CVF Conference on Computer Vision and Pattern Recognition*, pages 6966–6975, 2019.

W. Rahman, M. K. Hasan, S. Lee, A. Zadeh, C. Mao, L.-P. Morency, and E. Hoque. Integrating multimodal information in large pretrained transformers. In *Proceedings of the conference. Association for Computational Linguistics. Meeting*, volume 2020, page 2359. NIH Public Access, 2020.

D. Ramachandram and G. W. Taylor. Deep multimodal learning: A survey on recent advances and trends. *IEEE signal processing magazine*, 34(6):96–108, 2017.

S. Sankaran, D. Yang, and S.-N. Lim. Multimodal fusion refiner networks, 2021.

M. Sardelich and S. Manandhar. Multimodal deep learning for short-term stock volatility prediction. *arXiv preprint arXiv:1812.10479*, 2018.

S. Shankar. Neural dependency coding inspired multimodal fusion. *arXiv preprint arXiv:2110.00385*, 2021.

S. Shankar, E. Breck, and J. Atwood. Assessing representation issues in developing world data. 2017.

K. Simonyan and A. Zisserman. Two-stream convolutional networks for action recognition. In *Proceedings of the Neural Information Processing Systems (NIPS)*, 2015.

S. Siriwardhana, A. Reis, R. Weerasekera, and S. Nanayakkara. Jointly fine-tuning" bert-like" self supervised models to improve multimodal speech emotion recognition. *arXiv preprint arXiv:2008.06682*, 2020.

K. Sohn, W. Shang, and H. Lee. Improved multimodal deep learning with variation of information. *Advances in neural information processing systems*, 27:2141–2149, 2014.

J. Sui, T. Adali, Q. Yu, J. Chen, and V. D. Calhoun. A review of multivariate methods for multimodal fusion of brain imaging data. *Journal of neuroscience methods*, 204(1):68–81, 2012.

M. Suzuki, K. Nakayama, and Y. Matsuo. Joint multimodal learning with deep generative models. *arXiv preprint arXiv:1611.01891*, 2016.

S. Taheri and Ö. Toygar. Animal classification using facial images with score-level fusion. *IET computer vision*, 12(5):679–685, 2018.

R. Taori, A. Dave, V. Shankar, N. Carlini, B. Recht, and L. Schmidt. Measuring robustness to natural distribution shifts in image classification. *arXiv preprint arXiv:2007.00644*, 2020.

Y.-H. H. Tsai, S. Bai, P. P. Liang, J. Z. Kolter, L.-P. Morency, and R. Salakhutdinov. Multimodal transformer for unaligned multimodal language sequences. In *Proceedings of the conference. Association for Computational Linguistics. Meeting*, volume 2019, page 6558. NIH Public Access, 2019a.

Y.-H. H. Tsai, P. P. Liang, A. Zadeh, and L.-P. Morency. Learning factorized multimodal representations. *arXiv preprint arXiv:1906.0617*, 2019b.

L. Turchet, C. Fischione, G. Essl, D. Keller, and M. Barthet. Internet of musical things: Vision and challenges. *IEEE Access*, 6:61994–62017, 2018.

P. K. Varshney. Distributed bayesian detection: Parallel fusion network. In *Distributed Detection and Data Fusion*, pages 36–118. Springer, 1997.

V. Vielzeuf, A. Lechervy, S. Pateux, and F. Jurie. Centralnet: a multilayer approach for multimodal fusion. In *Proceedings of the European Conference on Computer Vision (ECCV) Workshops*, pages 0–0, 2018.

W. Wang, D. Tran, and M. Feiszli. What makes training multi-modal classification networks hard? In *Proceedings of the IEEE/CVF Conference on Computer Vision and Pattern Recognition*, pages 12695–12705, 2020a.

X. Wang, R. Girshick, A. Gupta, and K. He. Non-local neural networks. In *Proceedings of the IEEE conference on computer vision and pattern recognition*, pages 7794–7803, 2018.

Y. Wang, Y. Shen, Z. Liu, P. P. Liang, A. Zadeh, and L.-P. Morency. Words can shift: Dynamically adjusting word representations using nonverbal behaviors. In *Proceedings of the AAAI Conference on Artificial Intelligence*, volume 33, pages 7216–7223, 2019.

Y. Wang, W. Huang, F. Sun, T. Xu, Y. Rong, and J. Huang. Deep multimodal fusion by channel exchanging. In *Advances in Neural Information Processing Systems (NeurIPS)*, 2020b.

M. Wöllmer, F. Weninger, T. Knaup, B. Schuller, C. Sun, K. Sagae, and L.-P. Morency. Youtube movie reviews: Sentiment analysis in an audio-visual context. *IEEE Intelligent Systems*, 28(3):46–53, 2013.

X. Yan, S. Hu, Y. Mao, Y. Ye, and H. Yu. Deep multi-view learning methods: A review. *Neurocomputing*, 448:106–129, 2021.

X. Yang, P. Molchanov, and J. Kautz. Multilayer and multimodal fusion of deep neural networks for video classification. In *Proceedings of the 24th ACM international conference on Multimedia*, pages 978–987, 2016.

A. Zadeh, M. Chen, S. Poria, E. Cambria, and L.-P. Morency. Tensor fusion network for multimodal sentiment analysis. *arXiv preprint arXiv:1707.07250*, 2017.

A. Zadeh, P. P. Liang, N. Mazumder, S. Poria, E. Cambria, and L.-P. Morency. Memory fusion network for multi-view sequential learning. In *Proceedings of the AAAI Conference on Artificial Intelligence*, volume 32, 2018a.

A. Zadeh, P. P. Liang, S. Poria, P. Vij, E. Cambria, and L.-P. Morency. Multi-attention recurrent network for human communication comprehension. In *Thirty-Second AAAI Conference on Artificial Intelligence*, 2018b.

A. B. Zadeh, P. P. Liang, S. Poria, E. Cambria, and L.-P. Morency. Multimodal language analysis in the wild: Cmu-mosei dataset and interpretable dynamic fusion graph. In *Proceedings of the 56th Annual Meeting of the Association for Computational Linguistics (Volume 1: Long Papers)*, pages 2236–2246, 2018c.

J.-Y. Zhu, T. Park, P. Isola, and A. A. Efros. Unpaired image-to-image translation using cycle-consistent adversarial networks. In *Proceedings of the IEEE international conference on computer vision*, pages 2223–2232, 2017.

A Overview of Fusion Techniques

Multimodal fusion has been a heavily researched area for decades [Osadciw and Veeramachaneni, 2009, Varshney, 1997]. Such models have been used for tasks ranging from video classification [Yang et al., 2016], action recognition [Cabrera-Quiros et al., 2019], and speech enhancement [Hou et al., 2017] to brain studies Sui et al. [2012], ecological applications [Taheri and Toygar, 2018], and monitoring systems [Varshney, 1997, Li and Seignez, 2018]. However most models have primarily focused either on architectural changes or designing new fusion layers [Yan et al., 2021].

Early Fusion Figure 1a illustrates a general early fusion scheme. Early fusion, sometimes also called feature fusion in the early literature [Ayache et al., 2006, Chair and Varshney, 1986], creates a multimodal representation by combining unimodal information before they are processed. One can broadly interpret an Early Fusion scheme as one that integrates unimodal features before ‘learning high level concepts’. Early fusion models have the ability to model highly complex dependencies between different modalities, however they generally face problems when dealing with heterogeneous sources such as text and images.

Late Fusion In contrast to early fusion, late fusion designs learn ‘high level semantic concepts’ directly from unimodal features. Late fusion allows an easy way to aggregate information from diverse modalities and can easily incorporate pre-trained models (e.g. Rahman et al. [2020]). As such, late fusion has been the more commonly utilized framework for multimodal learning [Ramachandram and Taylor, 2017, Simonyan and Zisserman, 2015]. However, late fusion models, illustrated in Figure 1b, run the risk of missing cross-modal interactions in the mixed feature space.

Architecture Changes Due to the wide variety of applications and tasks which require multimodal fusion, over the years a plethora of different architectures have been used. Some of the recent works include that of Vielzeuf et al. [2018], Sankaran et al. [2021], Pérez-Rúa et al. [2019], Hazarika et al. [2020], and Khan et al. [2012]. Vielzeuf et al. [2018] proposed a multimodal fusion design called CentralNet that is based on aggregative multi-task learning. Sankaran et al. [2021] bring together ideas from CentralNet and Cycle-GAN [Zhu et al., 2017] and design a Refiner Fusion Network (Refnet). The Refnet design uses a de-fusion model trained via cyclic losses to align both unimodal and multimodal representations in a common latent space. Pérez-Rúa et al. [2019] used neural architecture search to find a good architecture for convolutional networks. The discovered architecture is a multistep fusion model that fuses information from different individual unimodal layers multiple times. Hsu and Glass [2018] and Khattar et al. [2019] used ideas from unsupervised learning to use multimodal autoencoders to learn better representations. Tsai et al. [2019b] improved upon the factor model based approach of Hsu and Glass [2018] by incorporating prior matching and discriminative losses. Nagrani et al. [2021] modify the multimodal transformer Tsai et al. [2019a] to incorporate bottlenecks.

Our proposed method, though technically an architecture change, is a single change that *treats the existing model as given*. It is closer in spirit to a black-box change, compared to the aforementioned methods. Hence it is *complementary* to this line of work. We experiment with many of the aforementioned models to show how our proposal consistently improves performance.

Fusion Techniques Other than basic fusion layers such as pooling and concatenation, other common layers use include aggregation [Khan et al., 2012], tensor factorisation [Liu et al., 2018], attention modules [Zadeh et al., 2018a, Tsai et al., 2019a], channel-swaps Wang et al. [2020b] and non-local gating [Hu et al., 2019, Wang et al., 2018, Liu et al., 2019]. Rahman et al. [2020] used pre-trained transformer [Siriwardhana et al., 2020] along with Wang et al. [2019] modulation gate to achieve state of the art results on the multimodal sentiment benchmarks MOSI Wöllmer et al. [2013] and MOSEI Zadeh et al. [2018c]. LFN [Zadeh et al., 2017] combined information via pooling projections of high dimensional tensor representation of multimodal features. These works propose specific fusion techniques, they design specific forms of the F function (see Figure 1). Our proposed technique is *agnostic to the choice of the fusion function F* and thus is *orthogonal* to these ideas.

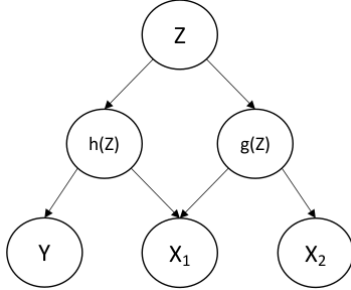
Model Agnostic Methods A number of alignment and information based losses have also been explored to improve fusion by inducing semantic relationships across the different unimodal representations [Abavisani et al., 2019, Bramon et al., 2011, Liang et al., 2021b, Liu et al., 2021, Han et al.,

2021]. These are purely train-time objectives and can be generally applied to most multimodal fusion models. Recently Wang et al. [2020a] proposed a new approach that can be applied to any multimodal architecture. Their approach called Gradient Blending (GB) tackles the problem of joint learning when different unimodal networks have varying capacity, by learning individual modality weights factors based on the model performances. Our proposal instead of adding losses or adding reweighting factors instead adds backprojective connections. So, these model-agnostic proposals are in general complementary to our approach, and can be *combined with it to achieve further improvements*.

B Further Experiments

B.1 Synthetic Experiments

We further explore the setting implied by the generative model described in Section 3.1. For this we generate data as from a generative model matching the dependencies in Figure 3. We set the function h to be leaky-Relu and g to be the sine function. We choose f such that $f \circ h$ is linear. Note that the specific choice of h, g makes the function $h + g$ non-invertible. Z was sampled from a uniform distribution on $[-2.5, 2.5]$ and all linear transform matrix were also sampled from the standard normal distribution. The specific generative equations are presented in the equations below.



$$\begin{aligned}
 Z &\sim \mathcal{U}[-2.5, 2.5]^d \\
 W_1 &\sim \mathcal{N}(0, I), W_2 \sim \mathcal{N}(0, I), W_y \sim \mathcal{N}(0, I) \\
 X_1 &= \text{IRelu}(W_1 Z) - 2 * |\eta| \sin(W_2 Z) + \epsilon_1 \\
 X_2 &= \sin(W_y Z) + \sigma_2 \epsilon_2 \\
 Y &= W_y Z + \epsilon_y
 \end{aligned}$$

Figure 7

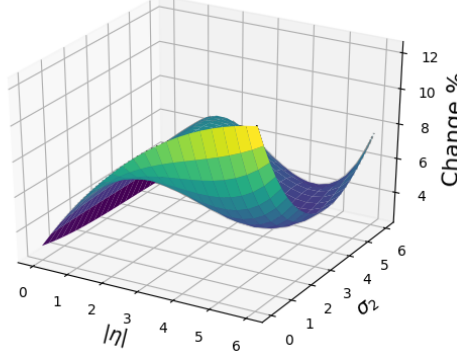


Figure 8: Percentage Improvement over varying levels of modality dependence. Note that this is percent improvement in MSE so higher is better

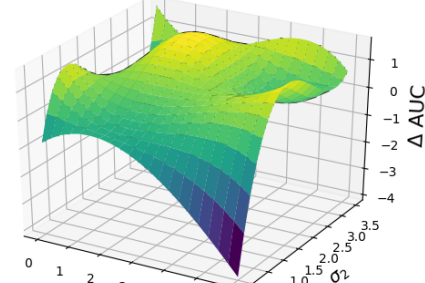


Figure 9: AUC change for pro-fusion model over normal fusion over varying levels of modality dependence. Since the metric is error, lower AUC is better

All noise terms ϵ are sampled from a standard normal distribution. We train a 3 layer MLP to solve this regression task. Fusion was done via plain concatenation of the second layer. For the pro-fusion model, the same fusion vector was linearly transformed and fed along with the input. We varied the strength η of corruption in X_1 and of σ_2 the noise in X_2 , and ran for each such value 30 trials. In close to 90% of all trials we found the pro-fusion model to perform better with an average improvement of 8%. We plot the contours for multiple different runs in Figures 8.

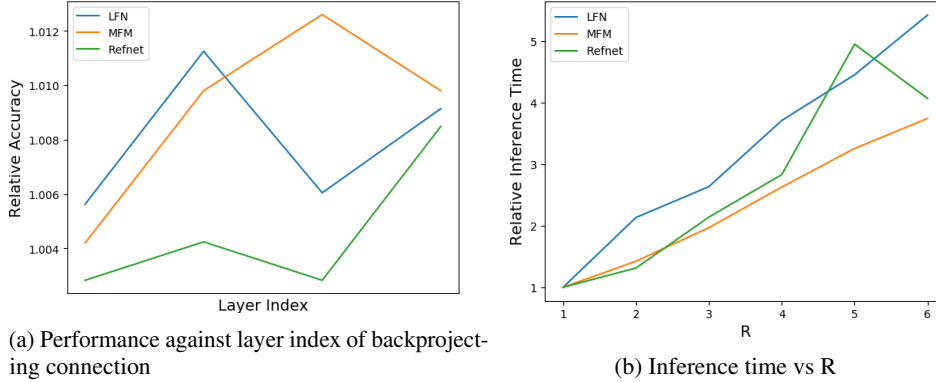
We also do robustness evaluation of this model over different values of noise parameters. We use the AUC (area under ROC curve) metric for this purpose. In Figure 9 we plot the improvement in AUC of the pro-fusion model over direct fusion against the different values of η/σ_2

B.2 Exploratory Experiments

In this section we explore various aspects of the backprojecting connections, such as the layer at which backprojecting connection joins, the number of unrolling steps and the inference complexity.

We measure the training time and inference time for pro-fusion with different architectures relative to that for the base model for different number of unrolling steps R . The straightforward way in which the current pro-fusion design uses the base model, suggests that both training and inference time should vary proportionately to the number of steps. This expectation is brought out in our experiments and can be seen in Figure 10b.

We also conduct experiments with determining at which upstream layer should the fused out should be connected back to. For this once again we run trials on the AVMNIST data. Our results are depicted in Figure 10a.



C Financial Data Details

The data itself is not licensed but following [Liang et al. \[2021a\]](#), [Sardelich and Manandhar \[2018\]](#) can be gathered from online records of historical stock prices and events.

- **FB** is composed of S&P 500 stocks which are part of food, meats and restaurant chains and includes the tickers CAG, CPB, DRI, GIS, HRL, HSY, K, MCD, MKC, SBUX, SJM, TSN, YUM.
- **HEALTH** is composed of following health-care and pharmaceutical sector tickers MRK, WST, CVS, MCK, ABT, UNH, TFX, PFE, GSK, NVS, WBA.
- **TECH** is composed of technology and information service stocks from NASDAQ. We include tickers AAPL, ADBE, AMD, AMZN, GOOG, HPQ, IBM, INTC, MSFT, MSI, NVDA, ORCL, QCOM, ZBRA.

C.1 Robustness Computation

We use the area under the performance-noise curve as the measure of robustness. This measure of robustness is the same as the one used by [Liang et al. \[2021a\]](#), [Taori et al. \[2020\]](#), and can be computed via the following integral:

$$\text{ROBUSTAUC} = \tau = \int \text{Perf}(f, \sigma) - \text{Perf}(b, \sigma) d\sigma$$

where $\text{Perf}(., \sigma)$ is the performance metric evaluated on a dataset corrupted with noise level σ , f is the model to be evaluated and b is a baseline model. Basically, the model is evaluated on the same

dataset corrupted on an equally spaced grid of noise levels and the performance is averaged over all the noise configurations is used. Note that the *Perf* as used by [Shankar et al. \[2017\]](#), [Taori et al. \[2020\]](#) is a positive metric like accuracy. For inverse metrics like MSE one has to use the negative of the above integral. For computing robustness we our experiments we use a transformer model as the baseline.

D Experimental Details

In this section we present the total results of all the experiments. We include metrics such as CORR (pearson correlation) which were not reported in the main body. We also report the average deviation of the scores in these tables.

D.1 AUC Measures and Average deviation on Financial Data

| Model | | F&B | | HEALTH | | TECH | |
|----------------|------|---------------|-------------|---------------|-------------|---------------|-------------|
| | | MSE ↓ | ROBUSTAUC ↑ | MSE ↓ | ROBUSTAUC ↑ | MSE ↓ | ROBUSTAUC ↑ |
| EFLSTM | Base | 0.73 (0.03) | 0.35 | 0.308 (0.005) | 0.018 | 0.742 (0.006) | 0.027 |
| | Our | 0.70 (0.04) | 0.40 | 0.306 (0.003) | 0.029 | 0.738 (0.004) | 0.028 |
| LFLSTM | Base | 0.77 (0.05) | 0.29 | 0.331 (0.009) | 0.016 | 0.736 (0.006) | 0.028 |
| | Our | 0.73 (0.05) | 0.33 | 0.315 (0.007) | 0.026 | 0.737 (0.005) | 0.028 |
| GB | Base | 0.690 (0.04) | 0.39 | 0.318 (0.03) | 0.022 | 0.740 (0.006) | 0.029 |
| | Our | 0.688 (0.02) | 0.39 | 0.305 (0.003) | 0.035 | 0.738 (0.005) | 0.029 |
| LF Transformer | Base | 0.838 (0.004) | 0.09 | 0.337 (0.004) | 0.012 | 0.757 (0.005) | 0.027 |
| | Our | 0.788 (0.004) | 0.15 | 0.331 (0.004) | 0.015 | 0.755 (0.005) | 0.028 |
| MulT | Base | 0.814 (0.005) | 0.13 | 0.333 (0.004) | 0.001 | 0.763 (0.005) | 0.025 |
| | Our | 0.765 (0.006) | 0.19 | 0.329 (0.005) | 0.002 | 0.757 (0.004) | 0.026 |
| EF transformer | Base | 0.836 (0.009) | 0. | 0.335 (0.001) | 0. | 0.755 (0.004) | 0. |
| | Our | 0.827 (0.009) | 0.01 | 0.326 (0.004) | 0.02 | 0.750 (0.004) | 0.00 |

Table 4: Results on stock prediction on the three sectoral datasets. The performance is evaluated on the Mean Squared Error (MSE) and ROBUSTAUC metric. Note we have already flipped the AUC sign for the inverse metric.

Our results on financial time-series prediction, while qualitatively similar to results of [\[Liang et al., 2021a\]](#), is different because of using more number of target stocks and different time period. For completeness we also report the error on the dataset provided by them in Table 5.

D.2 Multimedia

Complete results on AVMNIST along with the standard deviations of the performance are reported in Table 7

D.3 Hyperparameter Details

For the AVMNIST dataset, we used LeNet style unimodal feature generators. For the image encoder we used a 4 layer network with filter sizes [5,3,3,3] and max-pooling with width of 2. For the audio encoder the networks was a 6 layer networks with filter sizes [5,3,3,3,3,3] and max-pooling of width 2. The channel width was doubled after each layer. For GB models, the validation size was 0.8 and the model is fine-tuned for gradient blending for 30 epochs. For the optimization process we tried

Table 5: Results on multimodal dataset of [Liang et al. \[2021a\]](#) in the finance domain

| Dataset Metric | F&B MSE ↓ | | HEALTH MSE ↓ | | TECH MSE ↓ | |
|----------------|-----------|-------|--------------|-------|------------|-------|
| | Base | Our | Base | Our | Base | Our |
| EF-LSTM | 1.836 | 1.753 | 0.521 | 0.511 | 0.119 | 0.124 |
| LF-LSTM | 1.891 | 1.786 | 0.545 | 0.522 | 0.120 | 0.121 |
| LF-Transformer | 2.157 | 2.112 | 0.572 | 0.566 | 0.143 | 0.144 |
| MulT | 2.056 | 2.032 | 0.554 | 0.553 | 0.135 | 0.132 |

| | $Acc_7 \uparrow$ | $Acc_2 \uparrow$ | $MAE \downarrow$ | $CORR \uparrow$ |
|----------|-------------------|-------------------|------------------|-----------------|
| FLSTM | | | | |
| Base | 31.2 (0.5) | 75.9 (0.5) | 1.01 | 0.64 |
| Our | 31.8 (0.4) | 76.8 (0.3) | 1.0 | 0.66 |
| LFN | | | | |
| Base | 31.2 (0.4) | 76.6 (0.4) | 1.01 | 0.62 |
| Our | 32.1 (0.6) | 77.2 (0.2) | 1.01 | 0.62 |
| MAFBERT | | | | |
| Base | 40.2 (0.4) | 83.7 (0.3) | 0.79 | 0.80 |
| Our | 40.8 (0.4) | 84.1 (0.3) | 0.79 | 0.80 |
| MAGXLNET | | | | |
| Base | 43.1 (0.2) | 85.2 (0.4) | 0.76 | 0.82 |
| Our | 43.5 (0.3) | 85.5 (0.2) | 0.76 | 0.83 |
| MIM | | | | |
| Base | 45.5 (0.1) | 81.7 (0.2) | 0.72 | 0.75 |
| Our | 46.3 (0.2) | 83.4 (0.5) | 0.71 | 0.77 |
| | $Acc_7 \uparrow$ | $Acc_2 \uparrow$ | $MAE \downarrow$ | $CORR \uparrow$ |
| FLSTM | | | | |
| Base | 44.1 (0.2) | 75.1 (0.3) | 0.72 | 0.51 |
| Our | 44.8 (0.5) | 75.8 (0.3) | 0.72 | 0.52 |
| LFN | | | | |
| Base | 44.9 (0.3) | 75.3 (0.4) | 0.72 | 0.52 |
| Our | 46.1 (0.3) | 76.4 (0.3) | 0.71 | 0.52 |
| MAFBERT | | | | |
| Base | 46.9 (0.7) | 83.1 (0.4) | 0.59 | 0.76 |
| Our | 47.1 (0.7) | 83.6 (0.2) | 0.58 | 0.77 |
| MAGXLNET | | | | |
| Base | 46.7 (0.4) | 83.9 (0.3) | 0.59 | 0.77 |
| Our | 47.1 (0.3) | 84.2 (0.3) | 0.57 | 0.77 |
| MIM | | | | |
| Base | 53.3 (0.5) | 79.1 (0.3) | 0.59 | 0.71 |
| Our | 54.1 (0.8) | 80.1 (0.2) | 0.57 | 0.73 |

Table 6: Results on sentiment analysis on a) CMU-MOSI and b) CMU-MOSEI. Acc_7 , Acc_2 denote accuracy on 7, 2 classes respectively. MAE is Mean Absolute Error and Corr is the Pearson correlation.

random search on a logarithmic scale on the interval [1e-5, 5e-2]. We experimented with Adam, Adagrad, RMSProp, SGD optimizer with default configurations.

For the MFAS model, we did not do architecture search but instead used the final model presented by Pérez-Rúa et al. [2019]. That model is shown in Figure 11. While we have tried to stay close to the method described in Pérez-Rúa et al. [2019], Liang et al. [2021a] for creation of this dataset, our version of AVMNIST is potentially different from the earlier reported results as no standard dataset is available. For financial time series prediction, we used 128 dimensional RNNs. For transformers we used a 3 layer network with 3 attention heads. The sequence length used for BPTT in all cases was 750. The optimization process was chosen in a similar way as mentioned previously.

E Technical Analysis

Given a base model \mathcal{F} with input $x = (x_1, x_2, \dots, x_k)$, we want to create an augmented model $\hat{\mathcal{F}} : \mathcal{X} \times \mathbb{R}^d \rightarrow \mathcal{Y}$ with additional input $c \in \mathbb{R}^d$ such that $c = 0 \implies \hat{\mathcal{F}}(x, c) = \mathcal{F}(x)$. Recall that the function \mathcal{F} mentioned in Section 2.1 is given by $\mathcal{F}(x) = P(F(G_1(x_1), G_2(x_2), \dots, G_K(x_K)))$.

We create the desired network $\hat{\mathcal{F}}$ by providing c to the unimodal feature generators G_j . We use the output of the fusion layer F and project it back into the network as c_t via the matrix/function W_i . Specifically we choose a modified generator $\hat{G}_i : \mathcal{X}_i \times \mathbb{R}^{d_i} \rightarrow \mathcal{Y}$ to be given by $\hat{G}_i(x_i, c) =$

| Model | Accuracy \uparrow | |
|--------|---------------------|-------------------|
| | Base | Ours |
| LF | 71.4 (0.4) | 71.6 (0.4) |
| LFN | 71.1 (0.3) | 71.8 (0.3) |
| MFM | 71.4 (0.4) | 72.2 (0.6) |
| GB | 68.9 (0.6) | 69.3 (0.5) |
| Refnet | 70.6 (0.7) | 71.2 (0.5) |
| MFAS | 72.1 (0.5) | 72.5 (0.3) |

Table 7: Results on digit classification task with AVMNIST for various fusion architectures. The performance metric is Accuracy. Scores outside the average range of baseline models have been highlighted.

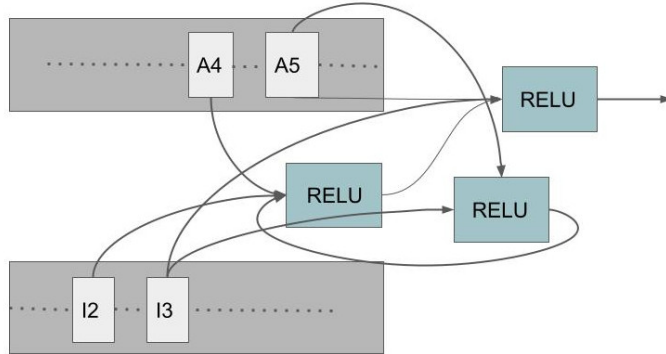


Figure 11: MFAS [Pérez-Rúa et al., 2019] based Multimodal Fusion Architecture for AVMNIST. Every arrow into the activation corresponds to a linear layer. The A4 and A5 represent the fourth and fifth layer of the audio encoder. Similarly I2 and I3 represent the second and third layer of the image encoder.

$G_j([x_i, W_i(c)])$, where W_i represents a matrix/network. This creates a recurrence relation which we unroll for R steps. The final vector c_R after R steps serves as the output of fusion which is then provided to the predictor model P .

Mathematically, we can write the overall operation as :

$$\begin{aligned}\hat{G}_i(x_i, c_{t-1}) &= G_j(x_i + W_i(c_{t-1})) \\ c_t &= E(F(\hat{G}_1(x_1, c_{t-1}), \dots, \hat{G}_K(x_K, c_{t-1}))) \\ \hat{Y} &= P(c_R)\end{aligned}$$

with the initial value $c_0 = \vec{0}$. We would like to draw the readers attention to the lack of $[t]$ subscript on the inputs x in Equation E above. This is because the iterations on t are on a dimension unrelated to any sequentiality in the input. Instead the model iteratively modifies its late-fusion features output, and makes it available to the unimodal network processing models/early stage features via the vector c_t . This is different from models like [Zadeh et al., 2018a] which use memory to store fusion vectors across different time-steps in the input, i.e. their networks processes x_t to produce fusion output.

E.1 Linear Model

Consider a simple linear model with multiple outputs and two input modalities. The two modalities are each \mathbb{R}^D and the number of outputs is K . We consider the late and early fusion model of Figure 12 with only 1 layer between the input and fusion and from fusion to output. We take the fusion layer F to be a concatenating operation. While the figure includes non-linearity, we will in this discussion look at the linear case.

Analysis The early fusion model works by concatenating the two inputs together, a linear transform to \mathbb{R}^{2d} followed by another transform to \mathbb{R}^K . On the other hand the late fusion model corresponds to two modality wise transform to \mathbb{R}^d which are then concatenated and transformed to \mathbb{R}^K . Note that in either case the second transformation is a $2d \times K$ matrix.

$$\begin{bmatrix} F_{11} & F_{12} \\ F_{21} & F_{22} \end{bmatrix} \begin{bmatrix} W_{11} & W_{12} \\ W_{21} & W_{22} \end{bmatrix} \begin{bmatrix} X_1 \\ X_2 \end{bmatrix} = \begin{bmatrix} F_{11}W_{11} + F_{12}W_{21} & F_{11}W_{12} + F_{12}W_{22} \\ F_{21}W_{11} + F_{21}W_{22} & F_{21}W_{12} + F_{22}W_{22} \end{bmatrix} \begin{bmatrix} X_1 \\ X_2 \end{bmatrix}$$

Late fusion on the other hand is expressible in the same formula by zeroing the off diagonal terms of W

$$\begin{bmatrix} F_{11} & F_{12} \\ F_{21} & F_{22} \end{bmatrix} \begin{bmatrix} W_{11} & 0 \\ 0 & W_{22} \end{bmatrix} \begin{bmatrix} X_1 \\ X_2 \end{bmatrix} = \begin{bmatrix} F_{11}W_{11} & F_{12}W_{22} \\ F_{21}W_{11} & F_{22}W_{22} \end{bmatrix} \begin{bmatrix} X_1 \\ X_2 \end{bmatrix}$$

First note that the rank of the effective matrix in early fusion is necessarily higher than that in late fusion. However even in cases when the rank of the effective matrix remains the same the matrix in late fusion is more constrained. To see this, consider a simple case where all F_{ij} are diagonal matrices; in which case the ratio between the rows in the top-left quadrant (i.e. $F_{11}W_{11}$) is the same as the one in the bottom-left quadrant (i.e. $F_{21}W_{11}$) (and the same is true for the other quadrants as well). Similar constraints hold more generally. For example take the case of $d = 1, D = 2, K = 2$. The net transformation in this case is a 4x2 matrix of the form:

$$\begin{bmatrix} f_{11}w_{11} & f_{11}w_{12} & f_{21}w_{21} & f_{21}w_{22} \\ f_{12}w_{11} & f_{12}w_{12} & f_{22}w_{21} & f_{22}w_{22} \end{bmatrix}$$

One can see that the ratio of the elements of the first column and second column is the same. The same holds for third and fourth columns. Evidently not all rank two 4x2 matrices are of this form. As such there are functions in the early fusion variant which cannot be expressed in the late fusion design.

Next we compare this to the pro-fusion design presented in this work. We use a variant where the concatenated late vector is projected back as an input to the input encoders 1c, and the entire network is unrolled once.

The composite action of the backward connection plus unrolling is still linear and is given by the following composition

$$\begin{bmatrix} F_{11} & F_{12} \\ F_{21} & F_{22} \end{bmatrix} \begin{bmatrix} W_{11} + G_{11}W_{11} & G_{12}W_{22} \\ G_{21}W_{11} & W_{22} + G_{22}W_{22} \end{bmatrix} \begin{bmatrix} X_1 \\ X_2 \end{bmatrix}$$

Note the presence of off-diagonal entries which similar to early fusion breaks the structure imposed by late fusion in the earlier case. However this model is not as expressive as early fusion as there can be some dependencies between the matrix entries.

E.2 Multiplicative Nonlinearity

While in the linear case, the extra freedom allowed by progressive fusion need not be very useful, the presence of multimodal interaction/ off-diagonal terms can have larger effects when dealing with non-linearity.

Lets take example of a multiplicative non-linear layer $H : \mathbb{R}^D \rightarrow \mathbb{R}^d$ with the ability to provide any d features obtained via pairwise multiplication of input features. For example for a vector input $[x_1, x_2, x_3, x_4]$ and output dimension $d = 3$, we can get any 3 of the 10 pairwise outputs i.e $[x_1^2, x_2^2, x_3^2, x_4^2, x_1x_2, x_1x_3, x_1x_4, x_2x_3, x_2x_4, x_3x_4]$. Using multiplicative non-linearity is useful for analysis as using the distributive property one can directly include behaviour of linear transformations. In Figure 12, we depict three simple non-linear fusion models with such non-linearity added in the layers. We denote the input features as X^1, X^2 for the two modalities, and their individual components are denoted by X_1^1, X_2^1, X_1^2 etc. We would also refer by $w^{p,q}$ the weight matrix applied on modality p in the layer q of the network.

Analysis After the first layer in the late-fusion design, the unimodal features are $\sum w_{ij}^{1,1} X_j^1$, $\sum w_{ij}^{2,1} X_j^2$ respectively. Then after the non-linearity, we get

$$\sum w_{ik}^{1,1} w_{il}^{1,1} X_k^1 X_l^1$$

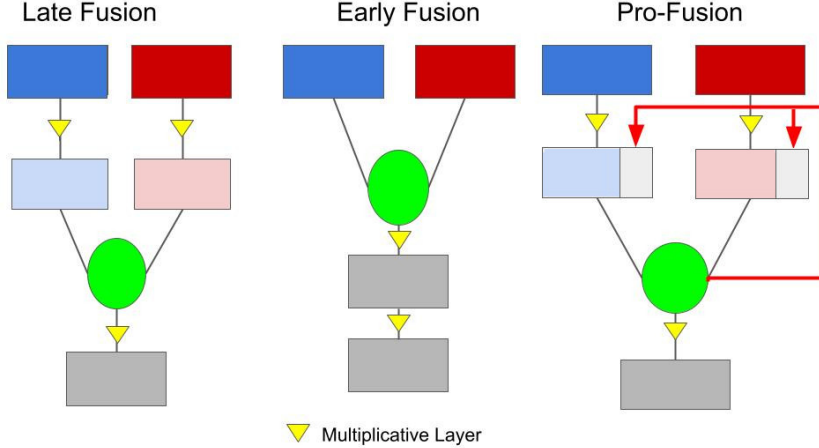


Figure 12: Representative Multimodal Fusion Architectures of Late fusion , Early fusion and Pro-fusion. The round green layer is the fusion layer (assumed to be concatenation). We also depict on the figure the location of multiplicative non-linearity with triangle, and highlight in red the back-projections of the pro-fusion design

These are then concatenated across modalities, and passed through another multiplicative non linearity. Hence the features obtained after this layer are given by

$$\sum w_{ik}^{1,1} w_{il}^{1,1} w_{i'm}^{2,1} w_{i'n}^{2,1} X_k^1 X_l^1 X_m^1 X_n^1$$

Effectively we have a linear combination of degree 4 terms that are symmetric in modalities i.e. $\{X_i^1 X_j^1 X_k^2 X_m^2, X_i^2 X_j^2 X_k^2 X_m^2, X_i^1 X_j^1 X_k^1 X_m^1\}$

However in the late fusion design the unimodal features are concatenated first, and then passed through the non-linearity. This produces after the first layer features of the form

$$w_{ij}^{1/2,1} X_i^{1/2} X_j^{1/2}$$

where $w^{1/2}$ and $X^{1/2}$ mean that choice over modalities 1 and 2 can be applied to w and X respectively. More simply one gets all pairwise terms from both modalities, instead of pairwise terms from only individual modalities. The next non-linearity, produces further multiplicative terms and we get linear combination of all degree 4 terms i.e. $X_i^{1/2} X_j^{1/2} X_k^{1/2} X_m^{1/2}$

Note here that no choice of linear operators between the layers can produce non-symmetric cross modal terms in the late fusion; and hence early fusion model has access to more features. On the other hand the first non-linearity in the early fusion case scales quadratically in the number of modalities. Specifically if the input dimensionality of each modality is D , and the number of modalities is n , then in early fusion the first non-linearity produces ${}^n D C_2$ feature outputs, whereas late fusion produces ${}^n D C_2$. In the next non-linearity where a second multiplicative pairing occurs, early fusion needs ${}^n D C_2 C_2$ parameters whereas late fusion needs ${}^n D C_2 C_2$. As such one might need many more samples to learn an early fusion model compared to a late fusion approach.

The back-projections of Pro-fusion model however alleviates the lack of feature diversity in late fusion. The back-projections provides access to some cross-modal features before the fusion layer. This allows pro-fusion access to any given single asymmetric degree 4 term; however due to the limited dimensionality of the backprojecting layer, not all combination of such degree 4 terms are accessible. For example if the backprojecting layer has size 2, then one can get only two pairs of independent asymmetric cross modal feature terms. Hence pro-fusion is more expressive pro-fusion but not as rich as early fusion.

F Training Backprojection layers

For training of backprojecting layers, we first build an augmented model $\hat{\mathcal{F}}$ by first extending the unimodal feature generators in the base model. Next we add the backprojecting networks W_i for each modalities. We pass the fused output to the unimodal generators through the backprojecting networks. Finally we fix a number of iterations, and unroll the model by applying the augmented network in a loop. The entire process is now differentiable, and autograd can compute the gradients.

```

1 # base model is assumed given in the layers
2 class FusModel(nn.Module):
3     def __init__(unimodal_layers, fusion_layer, hp):
4         self.unimodals = nn.ModuleList(*unimodal_layers)
5         self.fusion_layer = fusion_layer
6         self.num_modalities = len(unimodal_layers)
7
8     def forward(inputs):
9         uni_reps = [self.unimodals[_](inputs[_]) for _ in range(self.num_modalities)]
10        fused_rep = self.fusion_layer(uni_reps)
11
12    return fused_rep
13
14 class LateFusModel(nn.Module):
15     def __init__(unimodal_layers, fusion_layer, head, hp):
16         self.base_model = FusModel(unimodal_layers, fusion_layer, head, hp)
17         self.head = head
18         self.num_modalities = len(unimodal_layers)
19
20     def forward(inputs):
21         fused_rep = self.base_model(inputs)
22         return self.head(fused_rep)
23
24 class ProFusModel(nn.Module):
25     def __init__(num_modalities, unimodal_layers, fusion_layer, head, hp):
26         self.back_projecting_layers = nn.ModuleList([self.build_back_layers(unimodal_layers[i]),
27             fusion_layer.output_dim, hp) for i in num_modalities])
28         self.augmented_readers = nn.ModuleList([self.extend_layer(unimodal_layers[i], hp) for
29             i in num_modalities])
30         self.model = FusModel(self.augmented_readers, fusion_layer, hp)
31         self.output_head = head
32         self.hp = hp
33
34     def forward(self, inputs):
35         context_t = torch.zeros([inputs[0].shape[0], self.context_size])
36         context_t = [self.back_projecting_layers(context_t) for _ in range(self.hp.
37             num_modalities)]
38         for _ in range(self.hp.num_unroll_steps):
39             context_t = model_out = self.model(inputs, context_t)
40             context_t = [self.back_projecting_layers(model_out) for _ in range(self.hp.
41             num_modalities)]
42
43     return self.output_head(model_out)
44
45 def train_epoch(model, optimizer, criterion, hp, train_loader):
46     for i_batch, batch_data in enumerate(train_loader):
47         modalities, tgt = batch_data
48         optimizer.zero_grad()
49         preds = model(modalities)
50         loss = criterion(preds, tgt)
51         loss += model.regularizer(hp)
52         loss.backward()
53         optimizer.step()

```

G Additional Ablations

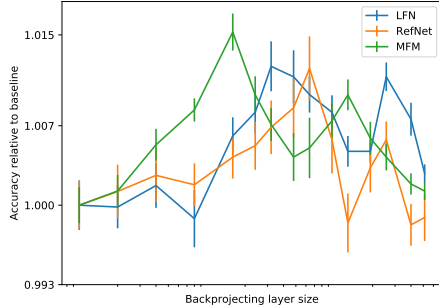


Figure 13: Relative accuracy of different models over varying dimensions of backprojecting connections. Each point corresponds to the normalized performance of the corresponding model when the hidden dimension is set to the values of on the x axis.

| Model | Accuracy \uparrow | | |
|--------|---------------------|-------------|-----------|
| | Base | Ours | Iterative |
| LFN | 71.1 | 71.8 | 71.5 |
| MFM | 71.4 | 72.2 | 69.9 |
| GB | 68.9 | 69.3 | 69.2 |
| Refnet | 70.6 | 71.2 | 70.7 |

Table 8: Results on digit classification task with AVMNIST for various fusion architectures. The performance metric is Accuracy, and was measured on five trials.

To assess the impact of multimodal backprojecting connections in the Pro-fusion approach against vanilla iterative models, we conduct experiments on AVMNIST. We use the baseline model, and change the unimodal feature generators to an iterative model. Effectively these models are similar to the Pro-fusion model except that the backprojections connect the output features of the unimodal feature generators to their inputs (See Figure ?? for an example). This allows us to distinguish between the effect of multimodal backprojection from the effect of generic iterative processing. We fixed the number of iterative steps to 2 (same as our ProFusion models) and ran 8 trials for these alternate iterative model. Our results along with baseline and Pro-fusion models are reported in Table 8

We can see from the results that while iterative models do lead generally to some improvement over the baseline models, Pro-fusion is still better. Moreover in some cases (like MFM) iterative models can be worse than the baseline. The key difference between a vanilla iterative model and pro-fusion based approach is that pro-fusion allows unimodal feature generators access to information from other modalities. As such unimodal feature generators can now produce features conditioned on the other modalities. On the other hand in the alternate approach, the unimodal features are blind to the features from alternate modalities. This is not very surprising if one look at this from the perspective of the graphical model in Figure 7. A standard message passing routine [Koller and Friedman, 2009] on the aforementioned graph, will have the message from X_2 effecting the belief of target Y via two paths: a) one along $X_2, g(Z), Z, h(Z)$ and the other along $X_2, g(Z), X_1, h(Z)$. Notice that along this second path, message from the modality X_2 is received at X_1 before further processing. If we interpret message creation as similar to feature generation, then this path makes features from modality X_2 available to the feature generator of X_1 , which is exactly what the backprojection layer also accomplishes. One caveat here is that unlike this example, in general we do not know which way to route the messages (as the dependence graph maybe unknown). As such in our proposal we treat all modalities symmetrically and re-cycle information through all of them.

We also run experiments to evaluate the effect of the dimensionality of the backprojecting connections. Notice that the input dimensionality to the backprojecting layer is fixed, and determined by the baseline model. We adjust the dimensionality of the backprojecting connection W , upto 512 and evaluate multiple models on the AVMNIST dataset. One might expect that backprojections with very low dimensions will be similar to baseline models with no backward connection. On the other hand with a high dimensionality in the backward connection, one runs into the same problem as early fusion of high parametric complexity. This expectation matches the empirical results, as can be seen in Figure 13, where we plot the accuracy (and standard error) of multiple models with varying backprojection sizes. Notice that for comparability across models, we have normalized all curves with their respective baseline results.